Journal of Applied Pharmaceutical Science Vol. 14(08), pp 216-229, August, 2024
Available online at http://www.japsonline.com
DOI: 10.7324/JAPS.2024.180236
ISSN 2231-3354

Optimization and characterization of hyper cross-linked cyclodextrins for improved efinaconazole delivery: A comprehensive study

Rudroju Anusha[1,2], Mothilal Mohan[2]*

[1]Teegala Ram Reddy College of Pharmacy, Meerpet-500097, Hyderabad, India.
[2]Department of Pharmaceutics, SRM College of Pharmacy, SRMIST, Kattankulathur, India.

ARTICLE HISTORY
Received on: 06/03/2024
Received on: 23/06/2024
Available Online: 05/08/2024

Key words:
NS, carbonate linking, encapsulation, photostability, permeation.

ABSTRACT

This study optimized cyclodextrin (NS) for controlled efinaconazole release in topical hydrogels. Utilizing Taguchi statistical design, key factors such as reaction time, temperature, stirring speed, and solvent volume were optimized. Efinaconazole was loaded into the polymers, forming inclusion complexes confirmed by FTIR, differential scanning calorimetry, and X-ray diffraction analyses. Hydrogel formulation was achieved using Carbopol 934. Optimized conditions were reaction time (480 minutes), temperature (100°C), stirring speed (3,000 rpm), and solvent volume (100 ml). Plain NS had an average particle size of 141–160 nm, while efinaconazole-loaded nanosponges ranged from approximately 69–84 nm. *In-vitro* release studies showed significantly enhanced release from nanosponge complexes compared to pure drugs. EFNS6, with controlled release, was chosen for further investigation to formulate a topical hydrogel due to its effective regulation of efinaconazole release. NS protected efinaconazole from photodegradation and prevented its chemical degradation over 6 months. *In-vitro* skin permeation studies highlighted NS' potential to enhance efinaconazole delivery into skin layers.

INTRODUCTION

Efinaconazole is a potent antifungal drug used topically to treat nail infections caused by specific fungi. It inhibits a crucial enzyme in fungal cell membrane synthesis and demonstrates promising activity against various fungal species [1,2]. However, formulating efinaconazole into a safe, stable, and effective dosage form poses challenges. Its limited water solubility hinders the de velopment of suitable oral formulations, leading to potential issues with bioavailability and therapeutic efficacy [3]. The drug's chemical stability can be affected by environmental factors, necessitating careful formulation design to maintain stability throughout its shelf life [4]. Some formulations of efinaconazole may experience discoloration during storage, potentially raising concerns about product quality and patient acceptance [5]. Finding the right topical dosage form is crucial to facilitate drug penetration into the nail bed or affected area. To ensure patient comfort and compliance, topical formulations must minimize skin irritation and adverse reactions at the application site. Selecting the most suitable dosage form, such as a cream, gel, or solution, depends on factors like patient preference and ease of use [6].

Numerous approaches have been adopted to tackle issues concerning the solubility and stability of drugs, along with enhancing the efficacy of conventional antifungal agents. These strategies encompass a range of approaches, such as chemical alterations of antifungal agents, utilizing carriers with penetration enhancers, developing nanoformulations, and employing combined therapies involving physical methods such as iontophoresis, photodynamic therapy, and lasers [7,8]. The success of topical antifungal therapy relies on the drug's capability to penetrate the skin's outer layer [stratum corneum (SC)] and the duration of treatment [9].

*Corresponding Author
Mothilal Mohan, Professor, Department of Pharmaceutics, SRM College of Pharmacy, SRM Institute of Science and Technology, SRM Nagar, Kattankulathur 603203, Tamil Nadu, India.
Email: mothipharma78 @ gmail.com, mothilam @ srmist.edu.in

Cyclodextrins provide a solution for improving drug solubility and stability. Studies have demonstrated that encapsulating efinaconazole using sulphoalkylether cyclodextrin derivatives increases its aqueous solubility. Despite this advantage, the complex manufacturing process of cyclodextrin formulations can lead to higher production costs [10]. In the patent EP 0149197, pharmaceutical compositions were disclosed, utilizing inclusion complexes of efinaconazole with partially etherified β-cyclodextrin derivatives containing hydroxyalkyl groups [11].

Recent research has focused on hypercross-linked cyclodextrins (HCDs) as a promising drug delivery platform to overcome the limitations of conventional cyclodextrin formulations. HCDs are commonly referred to as (NS). These HCDs form three-dimensional networks, efficiently complexing more drug molecules than natural cyclodextrins [12]. They offer versatility in dosage form options, including creams, gels, ointments, solutions, and nanoparticles, enabling precise control over drug release rates, improved solubility, stability, and targeted delivery [13]. Moreover, HCDs protect labile drugs, reduce side effects, and address challenges related to solubility and penetration. Researchers and pharmaceutical companies continue exploring NS' potential to develop innovative and effective drug delivery systems for various therapeutic agents [14]. Studies have already shown the potential of NS to increase the solubility and stability of drugs like curcumin. The evolution of this technology holds promise to revolutionize drug delivery and enhance patient outcomes in diverse medical applications [15].

NS-based topical formulations offer an innovative drug-delivery approach for various skin-related conditions and diseases. These formulations provide multiple advantages, including improved drug stability, controlled release, and enhanced skin penetration [16]. NS-based hydrogel formulations combine the unique properties of NS with hydrogels, creating an innovative drug delivery system. The hydrogels' three-dimensional structure allows for the effective encapsulation of drugs, enabling controlled and sustained drug release, leading to enhanced therapeutic efficacy and better patient compliance [17]. Furthermore, NS offers the potential to enhance the solubility of drugs with low water solubility, thus aiding their absorption through the skin or targeted tissues [18]. NS-based hydrogels are also suitable for transdermal drug delivery, making them valuable alternatives when oral administration is not feasible. Furthermore, these hydrogels hold promise in tissue engineering applications, where they can serve as scaffold materials for tissue regeneration and repair [19,20].

The NS-based gel formulation is expected to enhance antifungal activity, leading to better treatment outcomes for fungal skin and nail infections. The optimized drug delivery and sustained release of efinaconazole in the formulation are anticipated to maximize its effectiveness against fungal pathogens, accelerating infection resolution and reducing recurrence risk. This research aims to develop a novel hydrogel that precisely controls efinaconazole release, improving therapeutic efficacy and patient compliance in fungal skin infection treatment. Additionally, the study may advance the understanding of how the cross-linking density of NS affects drug release in hydrogel systems, opening new avenues for controlled drug delivery in various applications.

MATERIALS AND METHODS

Materials

β-cyclodextrin (β-CD), Carbonyldiimidazole (CDI), and dialysis membranes (Sartorius cut off 12,000 Da) were obtained from Sigma-Aldrich Chemicals Private Limited (Bangalore, India). Efinaconazole was supplied by MSN Labs Ltd. (Hyderabad, India). Carbopol 934, N-methyl-2-pyrrolidone, Triethanolamine, and Propylene glycol, were sourced from S.D. Fine Chem. Pvt. Ltd. (Mumbai, India). Throughout the study, exclusively Milli-Q water from Millipore was utilized. The investigation employed analytical-grade chemicals and reagents.

Preparation and characterization of HCDs

Design of experiments

Taguchi design

The statistical optimization of synthetic variables was achieved using the Taguchi design. For this purpose, the L9 orthogonal array (OA) design was employed. The optimization of reaction temperature in***°C (A),*** reaction time in minutes (B), stirring speed in rpm (C), and volume of solvent in ml (D) for producing cross-linked polymers with reduced particle size and enhanced yield was conducted using Design Expert software (Stat-Ease V8.0.1).

During exploratory experiments, independent variable levels were selected based on the results of trial experiments. The optimization of formulation parameters using Taguchi's orthogonal L9 array involved nine formulations, where the molar concentration of both components was consistently maintained. Table 1 provides a comprehensive summary of the experimental configurations determined by the model. It showcases the outcomes linked to the dependent variables, specifically Y1 (Practical yield) and Y2 (Particle size). To identify the main parameters influencing particle size and practical yield, analysis of variance (ANOVA) was employed.

Data analysis

Various statistical parameters, such as regression coefficient and coefficient of variation, were utilized to analyze the data and evaluate the selected models. To assess the significant influence of each term on the target value ($p < 0.05$), ANOVA and the F test were employed for data examination. The optimal solution was determined by solving the differential equations derived from the final model.

Optimization of variables

The synthesis variable settings for achieving the desired response were determined using the desirability approach of numerical optimization. The approach was fine-tuned by setting limits on both dependent and independent variables. To validate the statistical experimental procedures, three additional confirmation

Table 1. The theoretical and observed values of different trials of taguchi design.

Run	A (Reaction temperature in°C)	B (Reaction time in minutes)	C (Stirring speed in rpm)	D (Volume of solvent in ml)	Y1-practical yield (%)			Y2-particle size (nm)		
					Actual value	Predicted value	S/N ratio (dB)	Actual value	Predicted value	S/N ratio (dB)
1	80	480	3,000	200	68.1	68.22	−36.66	189	196	−45.53
2	120	360	3,000	150	83.5	83.32	−38.43	169	167	−44.55
3	100	480	1,000	150	96.9	96.59	−39.72	352	353	−50.93
4	100	420	3,000	100	94.6	94.59	−39.51	142	136	−43.05
5	80	360	1,000	100	63.3	63.16	−36.03	316	322	−49.99
6	120	480	2,000	100	88.2	88.39	−38.91	213	212	−46.57
7	100	360	2,000	200	91.2	91.52	−39.2	272	272	−48.69
8	80	420	2,000	150	66.2	66.22	−36.42	242	243	−47.68
9	120	420	1,000	200	86.4	86.39	−38.73	390	382	−51.82

experiments were conducted, each involving different molar quantities of the components [21].

Preparation of hyper cross-linked cyclodextrins (HCDs)

HCDs were synthesized using CDI as the crosslinking agent, following a previously detailed method [22]. The synthesis process began with the dissolution of β-CD in DMSO. Subsequently, CDI was added to the solution. Under continuous stirring, the reaction mixture was refluxed at optimum conditions. Following the completion of the reaction, the product was subjected to purification by washing with excess water and soxhlet extraction using ethanol. The white powder obtained was then dried and finely ground into a powder. The finely pulverized powder was mixed in water, and the resultant colloidal fraction was collected. Subsequently, the colloidal fraction was subjected to lyophilization to yield the powdered (NS) using a Lyodel Laboratory Scale Freeze Dryer (FD-01, Delvac Pumps Pvt. Ltd.). Ten different iterations of HCDs were generated by modifying the molar ratio between β-CD and CDI.

Physicochemical characterization of HCDs

The assessment of HCDs included the analysis of diverse characteristics such as particle size, polydispersity index (PDI), and zeta potential. For particle size analysis, dynamic light scattering was employed, utilizing the 90 Plus particle sizer manufactured by Brookhaven Instruments Corporation, USA. The instrument used for particle size analysis also facilitated zeta potential measurements, with the incorporation of an additional electrode. To gain insights into potential alterations in the chemical structure of HCDs in comparison to the original β-CD, the FTIR spectra of β-CD and the 10 HCD variants were recorded. This analysis was executed using an FTIR spectrometer, specifically the Perkin Elmer system 2,000. Furthermore, X-ray diffraction (XRD) analysis was conducted on both β-CD and HCDs to explore changes in their crystalline or amorphous characteristics. This investigative approach was undertaken using a Huber Guinier camera G670 utilizing Bragg-Brentano geometry. XRD patterns were collected within the 2θ range of 2.5°C–60°C. The thermal behavior and properties of the samples were investigated through differential scanning calorimetry (DSC) analysis. This thermal examination was conducted using a Perkin Elmer DSC/7 differential scanning calorimeter, which was equipped with a TAC 7/DX instrument controller from Perkin-Elmer, headquartered in CT, USA. For an assessment of the nanosponge morphology, TEM images of HCDs were acquired. These images were captured using a Jeol, 120KV Transmission electron microscope integrated with a digital CCD camera EMSIS QUEMESA 11 MP CCD camera, operating at a magnification of 25,000×.

Efinaconazole loading into HCDs

To load efinaconazole into HCDs, the freeze-drying method was employed, following a previously outlined protocol [23,24]. Initially, the HCDs were dispersed in 50 ml of Milli-Q water while being stirred. Subsequently, an excess amount of the drug was introduced into the HCDs suspension. The mixture underwent 10 minutes of sonication, followed by continuous stirring for 24 hours. Following this, the suspensions underwent centrifugation at 2,000 rpm for 10 minutes, leading to the sedimentation of the uncomplexed drug, which settled as a residue beneath the colloidal supernatant. The colloidal supernatant was carefully collected and underwent freeze-drying under controlled conditions, specifically at a temperature of −20°C and a reduced operating pressure of 13.33 mbar. The obtained freeze-dried powder was thoroughly dried and then stored in a desiccator. The percentage of drug association was calculated using the formula 1.

$$Percent\ drug\ association = \frac{Weight\ of\ drug\ in\ HCDs}{Total\ weight\ of\ drug\ added} \times 100 \quad (1)$$

Characterization of efinaconazole loaded HCDs (EFNS)

The evaluation of EFNS characteristics encompassed parameters such as particle size, PDI, and zeta potential. Particle size analysis was executed using dynamic light scattering, employing the 90 Plus particle sizer by Brookhaven Instruments Corporation, USA. Additionally, the same instrument, augmented with an extra electrode, facilitated the measurement of zeta potential. The FTIR spectra of NS16,

efinaconazole, and EFNS were recorded to identify any changes or modifications in the chemical structure of EFNS compared to the plain efinaconazole. XRD analysis was conducted on NS16, efinaconazole, and EFNS to investigate any changes in their crystalline or amorphous nature, which could provide valuable insights into the structural characteristics. DSC analysis of NS16, efinaconazole, and EFNS was conducted to study the thermal behavior and properties of the samples. To assess the morphology of NS, TEM images of EFNS were obtained to assess the morphology of drug-loaded NS.

Drug dissolution study

For *in-vitro* drug dissolution studies, a multicompartment system with rotating cells and dialysis membranes (Sartorius membrane filter molecular weight cut-off of 12 kDa) was employed, consisting of six compartments (n = 6). The donor phase consisted of 20 mg of efinaconazole dissolved in 100 ml of pH 6.4 buffer, and the receptor phase employed the same buffer. At predefined time intervals (0.25, 0.5, 0.75, 1, 2, 4, 6, 8, 10, 12, 15, 18, and 24 hours), samples from the receptor phase were collected, suitably diluted, and analyzed for efinaconazole content using a UV spectrophotometer at a wavelength of 259 nm. Each experiment was carried out three times to ensure accuracy and consistency. The data obtained from the dissolution study were then fitted into different kinetic models to assess the drug release mechanism.

Preparation of hydrogel formulation of efinaconazole NS

In the formulation of the efinaconazole NS gel base, Carbopol 934 was employed as described in reference [25]. To prepare a uniform 1% w/w gel base, the polymer was initially soaked in water for 2 hours. It was then dispersed in distilled water using a magnetic stirrer to ensure a homogeneous mixture. Subsequently, 1% Triethanolamine, 2% N-methyl-2-pyrrolidone, and 2% w/w Propylene glycol were introduced and stirred into the gel base. Following this, the gel base was enriched with NS loaded with efinaconazole, aiming for a concentration of 10% w/w efinaconazole in the gel base, maintaining a drug-to-carrier ratio of 10:90. As a control, a formulation was prepared by simply adding free efinaconazole to the gel base.

Characterization of the hydrogel formulation

Determination of pH

The pH of the hydrogel formulations was assessed utilizing a digital pH meter. To begin, 0.25 g of the NS-based gel was precisely weighed and dispersed in 25 ml of filtered water [26]. Before conducting the pH measurements, the pH meter was calibrated using buffer solutions with pH values of 4.0, 7.0, and 9.0. The pH of the formulation was assessed in triplicate, and the mean values were calculated for further analysis.

Investigation of photodegradation

Photodegradation studies were carried out to assess the stability of the formulations under UVA light exposure in the wavelength range of 320–400 nm. Two distinct systems were investigated in this study: a Carbopol gel formulation containing a NS complex with encapsulated efinaconazole (10%, w/w), and a gel formulation with an equal quantity of plain efinaconazole as a control. The experimental procedure involved spreading a 40 mg portion of the test gels uniformly at the bottom of a beaker using a syringe. Subsequently, the beakers were exposed to the UVA lamp for 2 hours. Subsequently, upon completion of the exposure duration, the contents within the beakers were quantitatively transferred into 20-ml calibrated flasks. To ensure uniformity, they were then subjected to 15 minutes of sonication. The resulting samples were then adjusted to a final volume of 20 ml, filtered through 0.45 μm membrane filters, and prepared for analysis. The degree of photodegradation was assessed by comparing the peak intensity of efinaconazole in the samples exposed to irradiation with that of an equivalent quantity of formulations that were not exposed to light. To maintain result accuracy, each sample was meticulously prepared and subjected to analysis in triplicate [27].

Stability assessment

Stability assessments were carried out on the formulations employed in the photodegradation experiments. The formulations consisted of Carbopol gel, containing either free efinaconazole or efinaconazole encapsulated within NS (10%, w/w). These formulations were subjected to comprehensive stability testing. To ensure optimal conditions for stability assessment, all formulations were stored in sealed amber glass bottles, shielded from light, within an environment maintained at a temperature of 25°C ± 2°C and a relative humidity of 60% ± 5%. At specific intervals, aliquots of the formulations (approximately 40–50 mg) were withdrawn and placed in calibrated flasks, resulting in a final volume of 20 ml. These samples were subjected to sonication in methanol, followed by dilution to the appropriate volume. Subsequently, membrane filtration was employed to ensure the removal of any particulates, and the samples were then analyzed to determine the residual efinaconazole content. To enhance the reliability of the results, triplicate measurements were taken for each formulation at each designated time point [28].

Skin permeation study

Animals

In vitro permeation studies were conducted using Wistar Albino rats, which were 6 to 8 weeks old and weighed between 120 and 150 g. These rats were obtained from Vab Bioscience, Musheerabad, Hyderabad. The rats were accommodated in ventilated animal rooms, where the temperature was consistently maintained at 25°C, following a 12/12-hour light/dark cycle. They had unrestricted access to both food and water throughout the study period. To ensure the animal's adaptation to the new environment, a week-long acclimatization period was provided before the commencement of the study. All animal experiments adhered to the approved protocols of the Institutional Animal Ethics Committee of TRR College of Pharmacy, with approval number 1447/PO/Re/S/11/CPCSEA-67/A. These stringent ethical guidelines were observed to ensure the welfare and ethical treatment of the animals throughout the experimentation process.

Skin permeation and deposition studies (in-vitro)

In vitro skin permeation and deposition investigations were conducted employing Franz diffusion cells, each outfitted with an efficient diffusion area of 3.14 cm². Before conducting these experiments, anesthesia was administered to Wistar Albino rats using chloral hydrate, and the hair on their abdominal region was carefully shaved off using a razor. Skin samples, approximately 5 cm² in size, were then excised from both the left and right sides of the abdomen. These excised skin samples underwent a meticulous cleaning process to remove subcutaneous fat and connective tissue. A thorough examination ensured that there were no visible defects in these skin samples.

In the diffusion cells, the excised skin samples were firmly held between the donor and receptor chambers, with the SC positioned toward the donor chamber. A thin layer, weighing 0.02 g, of the test gel was uniformly spread over the surface of the SC, covering an effective diffusional area of 1 cm². In the receptor compartment, a solution of 20 ml physiological saline with a pH of 7.2, containing 1% Tween80, was introduced. The temperature in the diffusion cells was consistently held at 32°*C* ± 1°*C, while continuous stirring at 300 rpm was maintained throughout the experiment.* At specific time intervals (0.5, 1, 2, 4, 6, 8, 10, 12, or 24 hours), 0.5 ml of the receptor medium was collected and immediately replaced with an equal volume of fresh physiological saline solution. This was done to maintain the sink conditions required for the experiment. The concentration of efinaconazole within the collected samples was subsequently determined using High-Performance Liquid Chromatography (HPLC).

After 12 hours of exposure, we carefully cleaned the skin surfaces using distilled water to remove any excess formulation. The topmost skin layer, known as the epidermis, was then peeled off using cellophane adhesive tape to recover the efinaconazole that had been deposited on the SC. The removed skin was divided into smaller fragments and homogenized. Efinaconazole, which adhered to the tape, and any remaining amounts on the homogenized skin were extracted using methanol. The resulting solution was subjected to centrifugation at 4,000 rpm for 10 minutes, and the concentration of efinaconazole in the supernatant was determined using HPLC analysis [29,30].

Statistical analysis

Each experiment was repeated a minimum of three times for robustness. Statistical analyses were conducted using SPSS 12.0 software. The data are depicted as mean values accompanied by the standard deviation (mean ± S.D.), and statistical significance is denoted by a significance level of $p < 0.05$.

RESULTS AND DISCUSSION

Preparation of HCDs

HCDs have been synthesized using different techniques, including convective heating, ultrasound, and microwave-aided synthesis. Among these methods, convective heating has been the most popular for synthesizing HCDs. However, this technique can sometimes result in the formation of reticulate complexes with multiple organic molecules [31].

Optimizing factors in the synthesis process, such as temperature, pH, concentration, solvent, catalyst, time, and pressure, can be challenging and time-consuming due to complex parameter connections. To address this, a statistical experimental design approach was employed in this investigation and optimization focused on synthesis. The design of experiments allows for exploring factor effects efficiently and accurately with fewer trials, providing relevant information on how individual and interactive factors affect the process [32].

The Taguchi statistical design is particularly useful in screening numerous parameters with fewer tests and employs OAs and ANOVA for analysis. This method helps estimate factor effects on feature attributes and structure while considering variability to determine optimal settings. Statistical assessment and experimental design are more effective in identifying relevant factors and their interactions with fewer runs compared to one-factor-at-a-time research. Taguchi experimental designs are fractional factorial designs that estimate main effects, disregarding higher-order interactions in screening research [33].

During the preliminary screening, it was determined that reaction time, reaction temperature, stirring speed, and solvent volume were the key process parameters influencing the synthesis of HCDs. The variable ranges for these parameters were defined by varying the reaction temperature, duration, stirring speed, and solvent volume. Temperatures exceeding 130°C led to the creation of reticulates, whereas temperatures below 80°C were insufficient to generate NS. An experimental approach was used to create a model for optimizing the preparation of cyclodextrin NS based on early findings.

A Taguchi OA was employed to identify the parameters affecting the particle size and percent practical yield of HCDs. Fractional factorial Taguchi OAs reduced the number of trials required to obtain maximum data. A matrix with four variables and three levels each was established to predict practical yield and particle size. Utilizing the Taguchi array consisting of nine experiments, the optimal combination of variables was identified. Preliminary point estimates from thorough pre-optimization tests were used as input functions in the statistical model for greater precision in statistical inference. All trials were duplicated three times to improve reliability.

The variance of the practical yield and particle size distribution was estimated and reported through ANOVA. ANOVA tests helped identify the variables that had the most significant impact on the response parameters. *F*-values in the *F*-distribution indicated the significance of a variable's influence on response characteristics. By pooling control variables to error terms and increasing error freedom, ANOVA analyses provided valuable insights into the effects of factors on response parameters.

Table 2 summarizes the primary parameters influencing both the NS' yield and particle size. The practical yield represents the actual amount of the desired product obtained after accounting for losses during the synthesis process. The practical yield directly impacts the economic efficiency of the synthesis process. A high practical yield means less wastage of raw materials, reducing production costs. It allows researchers and manufacturers to adjust reaction conditions, reagent quantities, or purification methods to improve the overall efficiency of

Table 2. Statistical analysis of regression models – ANOVA.

Variation source	Sum of squares	df	Mean square	*F*-value	*p*-value	*R2*
Y1- Practical yield (%)						
Model	1317.67	4	329.42	4328.14	<0.0001	0.9998
A (Reaction temperature in °C)	1278.602	2	639.3011	8399.577	<0.0001	
B (Reaction time in minutes)	39.07556	2	19.53778	256.7007	<0.0001	
Residual	0.30444	4	0.07611			
Cor Total	1317.982	8				
Y2-Particle size (nm)						
Model	57895.78	4	14473.944	302.943	<0.0001	0.9967
C (Stirring speed in rpm)	52494.89	2	26247.44	549.3651	<0.0001	
D (Volume of solvent in ml)	5400.889	2	2700.444	56.52093	0.0012	
Residual	191.1111	4	47.77778			
Cor Total	58086.89	8				

df: Degrees of freedom.

the synthesis. When transitioning from laboratory-scale to industrial-scale production, understanding the practical yield is essential. Consistent and reproducible synthesis processes are critical in pharmaceutical manufacturing. Monitoring and optimizing the practical yield contribute to the reproducibility of the nanosponge synthesis, ensuring consistent product quality. Understanding the relationship between reaction conditions and practical yield allows for the optimization of the synthesis process [34]. For nanosponge yield, the Model *F*-value of 4328.14 signifies its significance, with noise accounting for only 0.01% of the "Model *F*-Values." Factors A and B play crucial roles, as they have *F* values greater than the identification value *F*, indicating their substantial influence on practical yield. Factors C and D, with higher "Prob > *F*" values, are considered insignificant and have been removed from the model to enhance its performance. The model's Predicted R^2 value of 0.9988 closely aligns with the Adjusted R^2 value of 0.9995, indicating a good fit. The "Adeq Precision" value of 162.589 confirms the model's effectiveness in navigating the design space. The influence of Factor A, representing reaction temperature, on practical yield is rooted in its impact on the cross-linking process. Elevated temperatures expedite cross-linking, fostering the creation of a stable network. This acceleration enhances the overall yield by facilitating the formation of a robust structure. Likewise, Factor B, corresponding to reaction time, significantly contributes to practical yield. The extended reaction time enables thorough cross-linking, optimizing the utilization of reactants and, consequently, resulting in a higher practical yield. The equation in terms of coded factors can be used to make predictions about the response for given levels of each factor. The model equation for the response practical yield is presented in equation 2.

$$Practical\ yield = 82.07 - 16.13\ A[1] + 12.17A[2] - 2.67\ B[1] + 0.3333\ B[2] \quad (2)$$

A[1] and A[2] represents minimum and maximum values of A

B[1] and B[2] represents minimum and maximum values of B

This equation represents the relationship between the practical yield and the levels of factors A and B in the experimental design, allowing for prediction and optimization of the practical yield based on the chosen levels of factors A and B.

For nanosponge particle size, the Model *F*-value of 302.943 indicates significance, with noise accounting for only 0.01% of the "Model *F*-Values." Factors C and D are particularly important, as they have *F* values greater than the identification value *F*, signifying their substantial influence on particle size. Factors A and B, with higher "Prob > *F*" values, are considered insignificant and were removed from the model. The predicted R^2 value of 0.9833 closely matches the Adjusted R^2 value of 0.9934, indicating a good fit. The "Adeq Precision" value of 47.748 indicates a favorable signal, demonstrating effective navigation of the design space by the model. Factor C, pertaining to stirring speed, plays a pivotal role in determining the particle size of cyclodextrin NS. The speed at which the reaction mixture is stirred significantly affects the distribution of reactants, impacting the size of the formed NS. Higher stirring speeds facilitate more efficient mixing, reducing the chances of agglomeration and leading to smaller particle sizes. Conversely, lower stirring speeds might result in inadequate mixing, potentially causing larger particle formation. Factor D, representing the volume of solvent, influences particle size through its impact on the overall reaction environment. A larger volume of solvent provides a more spacious medium for the reaction to occur. This can lead to better dispersion of reactants, potentially yielding smaller-sized NS. Conversely, a smaller volume might lead to a more concentrated environment, impacting particle size. The model equation for the response particle size is presented in equation 3.

$$Particle\ size = 253.89 + 98.78\ C[1] - 11.56\ C[2] - 30.22\ D[1] + 0.4444D[2] \quad (3)$$

C[1] and C[2] represents minimum and maximum values of C

D[1] and D[2] represents minimum and maximum values of D

This equation represents the relationship between the particle size and the levels of factors C and D in the experimental design, allowing for prediction and optimization of the particle size based on the chosen levels of factors C and D.

In Figure 1A, the residual versus projected response (practical yield) from the final model is presented, with a consistent response range variance. Figure 1B displays a comparison between predictions and actual data, showing a good match between the model and experimental results. Similarly, Figure 1C exhibits the residual *vs.* predicted particle size from the final model, with a constant response range variance. Figure 1D illustrates a comparison between predictions and reactions, revealing a robust agreement between the model and the experimental data.

In the context of Taguchi methodology, the signal-to-noise (S/N) ratio serves as a metric to gauge both the quality and deviation from the desired target value. In this context, "signal" refers to the mean value, while "noise" pertains to the standard deviation from the mean for the specific response parameter [35]. Equation 2 reveals the S/N ratio.

$$\frac{S}{N} = -10\log\left(MSD\right) \tag{2}$$

—Mean square deviation (MSD) of the response variable

MSD should be modest since S/N is big. Thus, MSD is defined differently for each parameter [36]. Equation 3 is used to calculate the mean squared deviation.

$$MSD = \frac{1}{n}\sum_{i=1}^{n} y_i^2 \tag{3}$$

'n' represents the number of experiments in the OA and "y_i" refers to the mean shrinkage percentage for the ith experiment.

This study employed an L9 (3^4) OA, characterized by 4 columns and 9 rows. The smaller the practical yield and particle size, the better the conditions. Table 1 demonstrates realistic yield and particle size S/N ratios. The orthogonal experimental design allows for parameter-level separation. The average S/N ratio and range (D = delta = S/Nmax S/Nmin) of each control factor at each level are computed.

In Table 3, the mean S/N ratio for each parameter level represents the practical yield. Notably, the highest values for reaction temperature and reaction time observed in Table 3 indicate their crucial role in determining the realistic yield. Similarly, Table 3 also presents the mean S/N ratio for each parameter level, which reflects the particle size. Here, the highest values for stirring speed and solvent volume highlight their significant influence on the particle size, indicating that the particle size is dependent on the solvent volume and stirring speed.

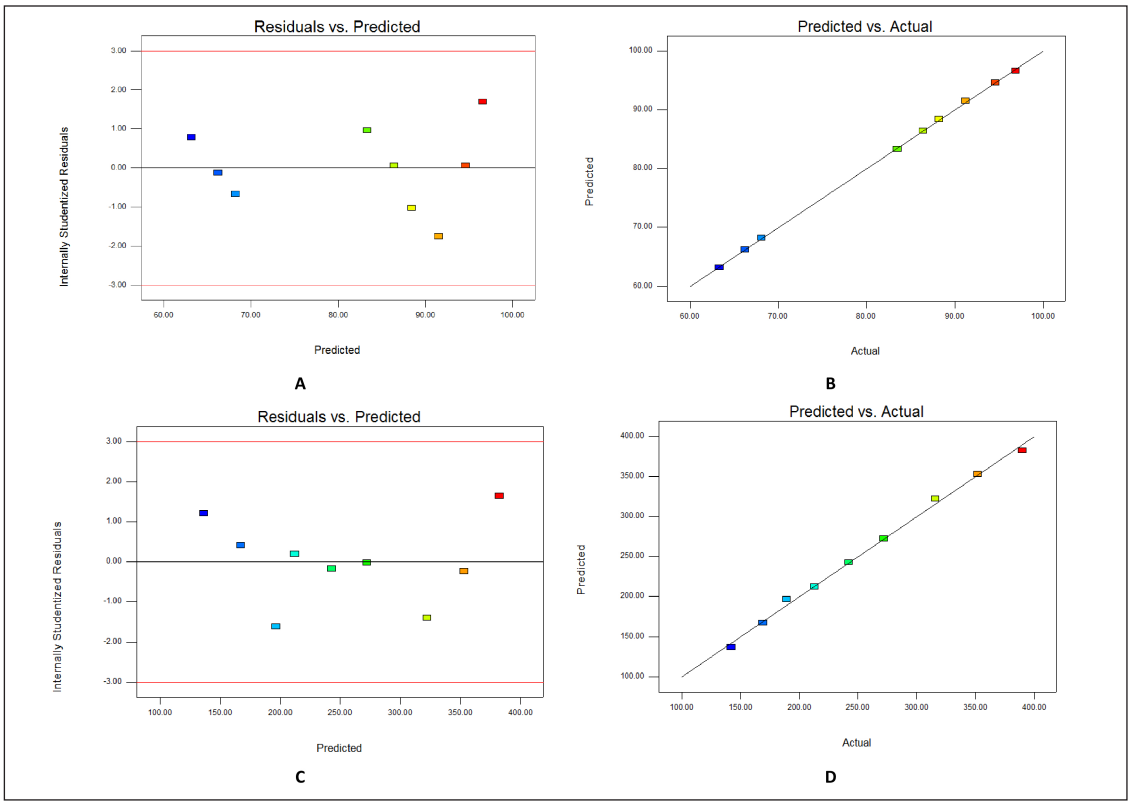

Figure 1. (A) Y1- Residuals versus predicted practical yield (B) Y1-Predicted versus actual practical yield (C) Y2- Residuals versus predicted particle size (D) Y2-Predicted versus actual particle size.

By employing numerical optimization with desirability, the NS was successfully formulated to achieve the desired responses. The main objective was to identify the optimal settings for independent variables, aiming to increase practical yield and decrease particle size. The outcomes of this optimization process are presented in Table 4, displaying the optimized and expected values for Y1 (practical yield) and Y2 (particle size).

To validate the obtained results, 10 batches of NS were prepared with varying molar concentrations of β-CD and CDI, ranging from 1:1 to 1:10. The comparison between the predicted values and the actual observations for Y1 and Y2 is presented in Table 4, indicating a close match between the two sets of data. This validation process has confirmed the reliability of the model used for optimization. Ultimately, through the comparison of predicted and experimental results, the optimal conditions for nanosponge synthesis were determined, leading to the achievement of the desired responses.

Characterization of HCDs

The laser light scattering analysis of NS demonstrated an average particle size ranging from 141 to 160 nm, characterized by a low PDI. The NS exhibited a high zeta potential, indicating the stability of the complexes and making them less prone to agglomeration. Figure 2A displays the FTIR spectra of β-CD and HCDs (NS1:1-NS1:10). Under optimal experimental conditions, HCDs exhibit a carbonate bond peak within the range of 1720–1750 cm^{-1}. In contrast, the FTIR spectra of β-CD, which acts as the precursor material for the NS, do not exhibit this peak between 1720 and 1750 cm^{-1}. Importantly, the NS presents distinctive peaks at 1026 cm^{-1} arising from the C-O stretching vibration of primary alcohol, at 2,918 cm^{-1} arising from the C-H stretching vibration, and at 1418 cm^{-1} arising from the C-H bending vibration. These distinctive peaks distinguish the NS (NS) from β-cyclodextrin. X-ray analysis was performed to elucidate the solid structure of the NS. Figure 2B shows the X-ray powder diffraction (XRPD)

Table 3. S/N values of both responses at different levels.

S.No.	Factor	S/N			
		low level	High level	Medium level	High-low
		Y1-Practical yield (%)			
1	A (Reaction temperature in°C)	−36.42	−38.98	−39.12	3.22
2	B (Reaction time in minutes)	−37.88	−38.22	−38.43	0.54
3	C (Stirring speed in rpm)	−38.16	−38.17	−38.2	0.04
4	D (Volume of solvent in ml)	−38.15	−38.19	−38.19	0.046
		Y2-Particle size (nm)			
1	A (Reaction temperature in°C)	−47.73	−47.55	−47.64	0.17
2	B (Reaction time in minutes)	−47.74	−47.51	−47.67	0.22
3	C (Stirring speed in rpm)	−50.91	−47.64	−44.37	6.53
4	D (Volume of solvent in ml)	−46.53	−47.72	−48.68	2.14

Table 4. Validation of design.

Factors	Nominal values	Predicted		Actual				
		Y1-Practical yield (%)	Y2-Particle size (nm)	Batch	Y1-Practical yield (%)	Y2-Particle size (nm)	PDI	Zeta potential (mV)
A (Reaction temperature in °C)	100	96.58	146.44	NS1:1	96.12	159.78 ± 3.6	0.28 ± 0.005	−23.45 ± 1.6
				NS1:2	95.78	141.28 ± 2.8	0.23 ± 0.005	−21.76 ± 1.9
				NS1:3	97.12	157.12 ± 3.8	0.19 ± 0.005	−24.65 ± 2.1
B (Reaction time in minutes)	480			NS1:4	96.54	158.38 ± 5.2	0.27 ±0.005	−23.68 ± 3.2
				NS1:5	96.72	149.73 ± 4.6	0.22 ± 0.005	−23.46 ± 1.4
				NS1:6	95.92	156.78 ± 3.7	0.28 ± 0.005	−22.32 ± 2.3
C (Stirring speed in rpm)	3,000			NS1:7	94.98	153.48 ± 2.6	0.18 ± 0.005	−24.12 ± 3.1
				NS1:8	95.89	146.32 ± 3.3	0.29 ± 0.005	−20.78 ± 2.5
D (Volume of solvent in ml)	100			NS1:9	96.35	148.76 ± 4.2	0.26 ± 0.005	−22.98 ± 1.9
				NS1:10	96.87	155.49 ± 3.5	0.24 ± 0.005	−24.08 ± 2.6

(The measurements were presented as the mean ± standard deviation, and each data point was obtained from a sample size of three).

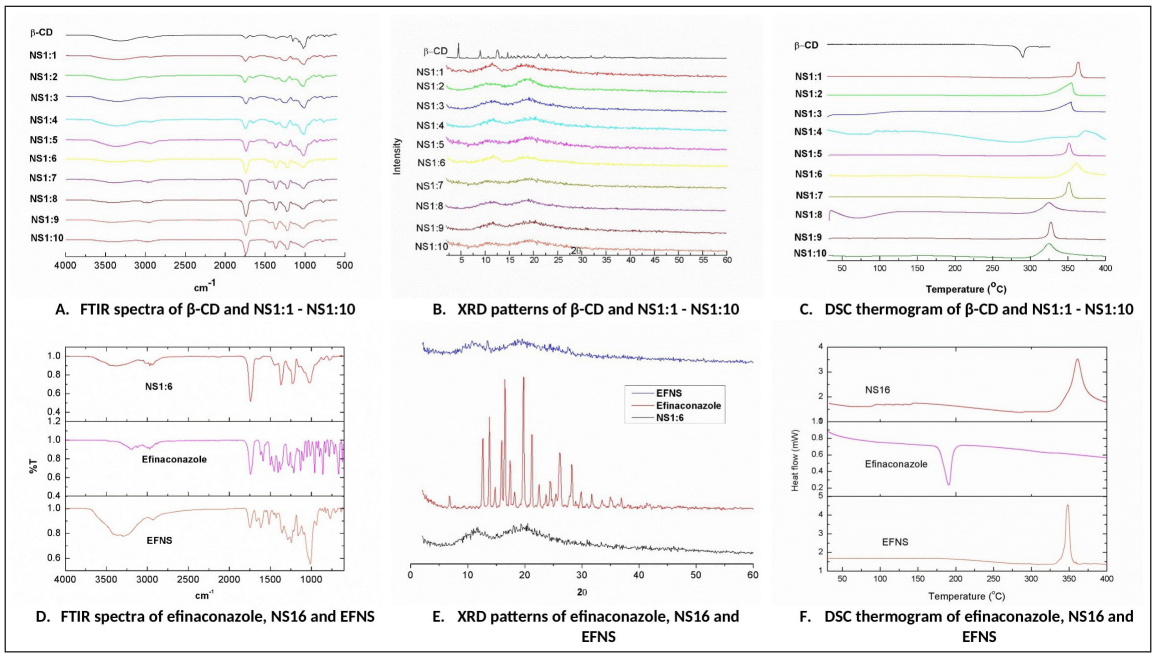

Figure 2. Results of FTIR, XRD, and DSC analysis.

study, displaying the crystalline structure of uncross-linked plain β-cyclodextrin. In comparison to the NS, the XRPD pattern of β-CD exhibits broad reflections as small peaks. The NS, on the other hand, displays few broad reflections, suggesting a paracrystalline structure. It is noteworthy that each batch of NS created with a specific cross-linking ratio exhibits identical diffraction patterns. Differential scanning analysis was carried out to provide a comprehensive characterization of the NS. In Figure 2C, the thermogram of β-CD is shown, displaying a distinct endothermic peak at 290°C, indicative of its melting temperature. In contrast, the NS exhibited no discernible DSC peak before reaching 350°C, indicating a remarkable level of thermal stability.

Preparation of efinaconazole loaded NS

NS pre-treated for drug loading resulted in nanoparticles with sizes below 150 nm. The freeze-drying method was used to load efinaconazole into distinct kinds of NS. Based on the specific type of NS utilized, the resulting drug-loaded NS formulations were designated as EFNS1 to EFNS10.

Characterization of efinaconazole-loaded NS

The analysis of particle size for efinaconazole-loaded nanosponges (EFNSs) indicated an average particle size ranging from approximately 69–84 nm, as detailed in Table 5. The PDI was notably low, denoting a tightly focused particle size distribution with minimal variability. This low PDI underscores the uniformity and consistency of the colloidal particles. Furthermore, the prominent zeta potential values suggest the potential for strong stability and a diminished tendency for particle aggregation. Notably, all formulated compositions exhibited a fine, free-flowing powder texture. This characterization was confirmed through TEM studies, illustrating that the basic spherical form and size of the plain NS were preserved even after drug encapsulation, as depicted in Figure 3. The particle size observed under TEM closely aligned with the measurements obtained through dynamic light scattering. Finally, the calculated percentages for drug loading and encapsulation efficiency for the developed efinaconazole NS are provided in Table 5.

The observed reduction in the size of the NS after loading with efinaconazole can be attributed to the intricate process of inclusion complex formation. Cyclodextrin NS, due to their unique structure and functional groups, are adept at forming inclusion complexes with guest molecules like efinaconazole. This process involves the accommodation of efinaconazole molecules within the cavities of the nanosponge network. Upon loading, the drug molecules interact with the cyclodextrin moieties through various forces such as Van der Waals, hydrogen bonding, and hydrophobic interactions. These interactions induce a structural rearrangement within the nanosponge matrix, causing it to contract or condense. The result is a more compact structure where the efinaconazole molecules are not merely adsorbed onto the surface but are intricately encapsulated within the three-dimensional network of the NS. This encapsulation serves several purposes. First, it enhances the stability of efinaconazole, shielding it from environmental factors that might degrade the drug. Second, it contributes to a more controlled release profile, as the drug is not exposed directly to the external environment but released gradually from the nanosponge matrix. Finally, the compact structure may also influence the overall physicochemical properties of the NS, such as their solubility and dispersibility [37]. Figure 2D presents a comparison of FTIR spectra between NS1:6 (NS), efinaconazole, and the efinaconazole-loaded nanosponges complex (EFNS).

Table 5. Characteristics of drug-loaded NS formulation.

Sample	Mean particle size ± SD (nm)	PDI	Zeta potential (mV)	Drug payload (%)	Encapsulation efficiency (%)
EFNS1	82.32 ± 2.89	0.24 ± 0.005	−27.76 ± 2.8	12.56 ± 0.89	53.98 ± 3.48
EFNS2	73.48 ± 2.54	0.27 ± 0.005	−25.67 ± 3.1	15.67 ± 1.32	64.98 ± 2.32
EFNS3	80.76 ± 1.87	0.23 ± 0.005	−29.67 ± 1.9	19.23 ± 1.76	71.24 ± 3.07
EFNS4	78.76 ± 3.12	0.25 ± 0.005	−26.79 ± 2.2	28.34± 2.09	77.86 ± 3.43
EFNS5	75.78 ± 2.43	0.21 ± 0.005	−28.76 ± 2.4	39.58 ± 2.17	83.45 ± 3.02
EFNS6	68.55 ± 2.35	0.26 ± 0.005	−24.75 ± 1.8	41.67 ± 1.78	86.93 ± 0.49
EFNS7	81.78 ± 1.98	0.28 ± 0.005	−20.98 ± 2.8	33.56 ± 2.32	89.34 ± 1.43
EFNS8	77.56 ± 3.02	0.23 ± 0.005	−27.12 ± 2.3	28.13 ± 1.65	80.56 ± 2.66
EFNS9	83.56 ± 1.78	0.29 ± 0.005	−23.67 ± 1.8	25.12 ± 0.96	74.12 ± 1.89
EFNS10	77.92 ± 3.15	0.19 ± 0.005	−22.34 ± 2.5	21.34 ± 0.76	70.56 ± 2.28

(The measurements were presented as the mean ± standard deviation, and each data point was obtained from a sample size of three).

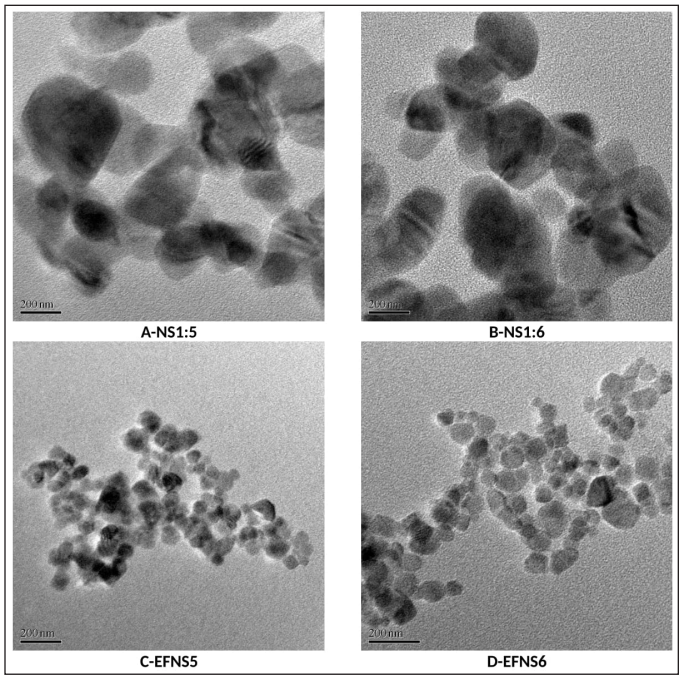

Figure 3. TEM images (A) NS1:5 (B) NS1:6 (C) EFNS5 (D) EFNS6.

The FTIR analyses unveiled indications of modest interactions between NS and efinaconazole, manifesting through the broadening and vanishing of drug peaks within the complex formations. A notable change was observed in the fingerprint region (900–1,400 cm^{-1}) of the FTIR spectra when comparing efinaconazole with the complex. The main characteristic peaks of efinaconazole were identified at approximately 3193.98, 3118.76, 3022.33, 2995.32, 2688.66, 1739.72, 1587.35, 1498.62, 1452.33, 1404.12, 1272.96, 1234.39, 1213.17, 958.58, 858.22, and 665.41 cm^{-1}. The characteristic peaks of efinaconazole displayed notable broadening or shifts within the formulations, underscoring evident interactions between efinaconazole and the NS.

To investigate the physical nature of efinaconazole within the cyclodextrin NS, XRD analysis was performed on pure efinaconazole, plain NNS6, and EFNS6. The results, as shown in Figure 2E, revealed distinctive characteristic peaks associated with efinaconazole, indicative of its prominent crystalline structure. Intriguingly, these characteristic peaks were notably absent in the EFNS6. The conspicuous absence of these crystalline peaks in EFNS6 strongly supports the inference that the drug is effectively encapsulated within the NS.

In Figure 2F, the DSC curves of three samples: free efinaconazole, plain NS6, and the efinaconazole nanosponges complex (EFNS6) were observed. The DSC spectra of efinaconazole display a distinct and sharp endothermic peak at 191.1°C, signifying its melting point. However, the DSC spectra of the NS exhibit exothermic peaks at approximately 350°C. Intriguingly, the efinaconazole complex also displays a broad exothermic peak around the same temperature of 350°C. Notably, for the formulations obtained through the freeze-drying process, the drug's endothermal peak is absent. This phenomenon strongly suggests interactions among the formulation components, indicating potential drug amorphization and/or the formation of inclusion complexes. The collective results from FTIR, DSC, and XRD studies definitively confirmed the presence of an inclusion complex between efinaconazole and the NS.

Figure 4A presents the dissolution profiles of both pure efinaconazole and the efinaconazole nanosponge complexes (EFNS1-EFNS10) in a simulated gastric medium. The results from *in-vitro* release studies showcase a substantial enhancement in the release rate of the complex when compared to the pure drug. The dissolution rate of pure efinaconazole remains relatively low, staying below 14% within 12 hours. In contrast, the nanosponge-encapsulated efinaconazole demonstrates a significantly faster and improved dissolution profile. The percentage of efinaconazole released from the nanosponge formulations after 12 hours shows a range between 64.54 and 99.68 %.

The diffusion of pure efinaconazole exhibited a mere 7% release within 120 minutes, while the drug encapsulated

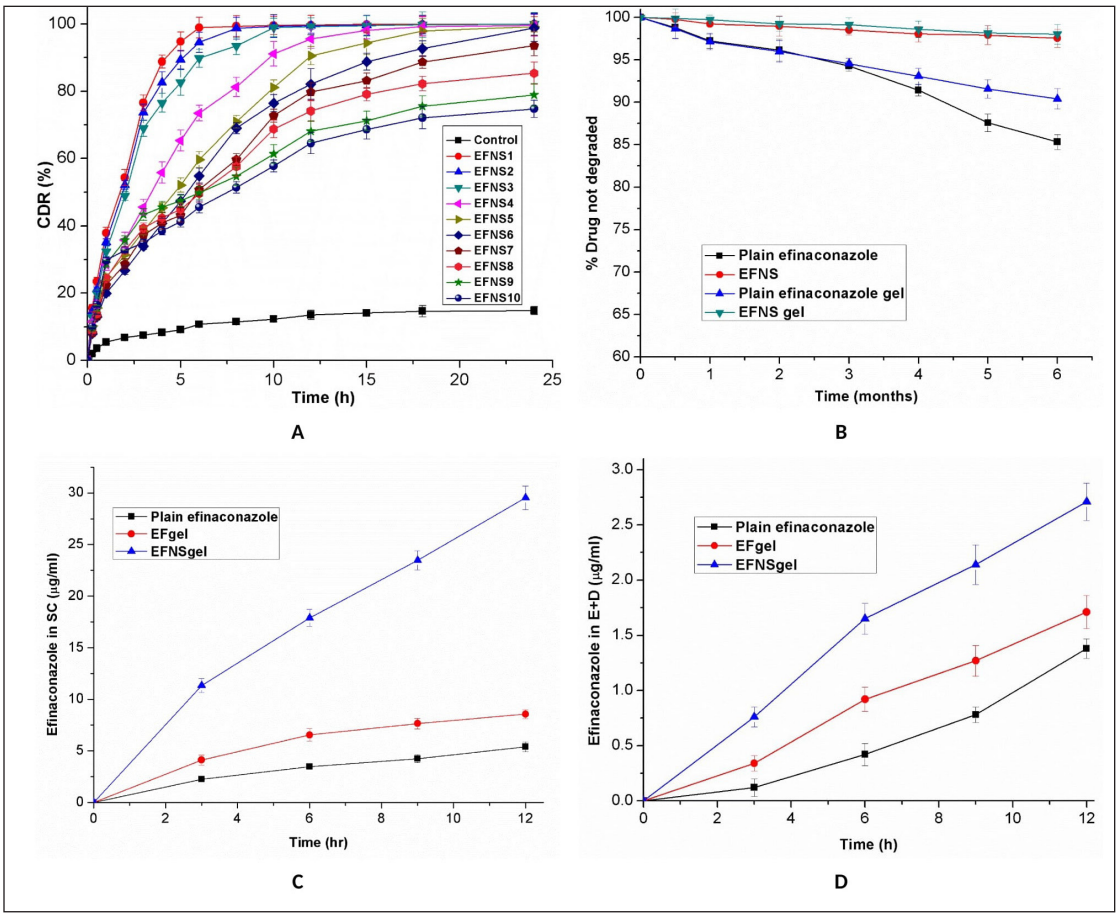

Figure 4. (A) Efinaconazole release from NS *in vitro* **(B)** Stability study results **(C)** *In-vitro* skin permeation of efinaconazole in gel and control in SC **(D)** *In-vitro* skin permeation of efinaconazole in gel and control in Epidermis and dermis.

in NS demonstrated a notably swifter release. Within the first 60 minutes, an average of 19.96%—37.89% efinaconazole was released, showcasing a rapid burst release phenomenon. This initial rapid release is commonly ascribed to the portion of efinaconazole that is either adsorbed or encapsulated as a non-inclusion complex on the surface of the NS. When the formulation is introduced into the release medium, this portion of efinaconazole swiftly diffuses into the surrounding liquid.

The maximum release of efinaconazole after 6 hours was observed in EFNS1 and EFNS2, reaching 98.89%–94.53%, respectively. In contrast, other NS exhibited a gradual reduction in release rate after this initial burst. This sustained and gradual release of efinaconazole can be ascribed to the diffusion of efinaconazole entrapped within the NS in the form of an inclusion complex, contributing to extended drug release over time.

EFNS3, EFNS4, EFNS5, and EFNS6 displayed a relatively modest burst effect and demonstrated more favorable sustained release properties upon drug loading. This behavior could be attributed to a higher proportion of efinaconazole forming an inclusion complex within the NS. Conversely, the relatively higher occurrence of non-inclusion complexation in EFNS1 and EFNS2 might be due to efinaconazole's limited access to the larger network of channels and pores within the structure. Additionally, the incomplete release of the drug from NS7 to NS10 could be attributed to the higher cross-linking density, which likely hindered the dissolution of the drug. Given the controlled release nature of EFNS6, it was selected for further investigation to formulate a topical hydrogel. The decision was based on its potential to regulate the release of efinaconazole effectively.

Efinaconazole gel formulation

Following literature guidance, the gel base formulation was developed by incorporating EFNS and utilizing Carbopol 934 polymer. Carbopol is a widely used base for topical preparations and is a hydrogel-forming polymer of acrylic acid. When in contact with water or alkaline solutions, the carboxyl groups in Carbopol hydrate, resulting in the formation of a hydrogel [16]. The formulation of EFNSincorporated Carbopol 934 hydrogel along with 2% w/w of Propylene glycol and 2% w/w of N-methyl-2-pyrrolidone as permeation enhancers. For gel neutralization, 1% w/w of Triethanolamine was employed. This approach mirrors a prior study that utilized a similar Carbopol hydrogel composition, leading to improved stability and permeation of Econazole nitrate [17]. Both formulations exhibited a pH ranging from 4.98–5.65, aligning with the skin's typical pH range of 3.0–9.0. This observation underscores the non-irritating nature of the preparation.

The photodegradation studies encompassed three variants: free efinaconazole, a Carbopol gel formulation incorporating free efinaconazole (EFgel), and l formulation embedding efinaconazole-loaded nanosponges (EFNSgel). These formulations were subjected to exposure under a UVA lamp possessing a wavelength range of 320–400 nm. This experiment aimed to quantify the extent of degradation that occurred due to the UVA irradiation. Upon exposure to the UVA lamp, the gel formulation containing pure efinaconazole experienced degradation of approximately 17.82% ± 1.26% of the drug. However, a significant reduction in the extent of efinaconazole. Photodegradation was observed in the formulations incorporating the NS-encapsulated efinaconazole. This outcome underscores the protective influence of the NS against Photodegradation. To assess whether the enhancement of efinaconazole Photostability was a result of the gel formulation, dedicated Photostability experiments were conducted using free efinaconazole. The outcomes revealed that when the drug was exposed directly to the UVA lamp, approximately 21.73% ± 2.08% of the drug experienced degradation. This finding suggests that the Carbopol gel formulation contributes to a degree of protection against photodegradation.

To further evaluate whether the NS contributed to the enhanced Photostability of efinaconazole and if this effect varied with time, additional photolysis experiments were conducted after the same formulations had been stored for 3 months at room temperature in the absence of light. This aspect aimed to mimic storage conditions that the formulations could undergo during practical use. The observed percentage loss of efinaconazole upon irradiation of the studied formulations is presented in Table 6. These results provide insights into the potential benefits of NS encapsulation in enhancing the Photostability of efinaconazole formulations.

To investigate the potential impact of NS on the chemical stability of efinaconazole, an extended aging study was conducted using the same formulations as those utilized in the photodegradation experiments. The formulations were subjected to analysis for 6 months, under controlled conditions of room temperature and darkness. The outcomes of this aging study are depicted in Figure 4B. During the 6 months, a degradation of approximately 14.68% was observed for free efinaconazole, while the gel formulation containing non-encapsulated efinaconazole experienced a degradation of approximately 9.6%. Strikingly, the formulations containing efinaconazole encapsulated within NS exhibited no significant decline in the efinaconazole content after the same duration of time. These findings underscore the protective capabilities offered by cyclodextrin NS, as they effectively prevent the chemical degradation of efinaconazole even under conditions that could potentially induce degradation. This observation further supports the potential advantages of utilizing NS encapsulation for enhancing the stability of pharmaceutical formulations.

Table 6. Photodegradation values for free and nanosponge encapsulated efinaconazole in gel formulations, immediately after preparation and after 3-month storage.

Sample	% efinaconazole degraded	
	Immediately after preparation	After 3-month storage
Free efinaconazole (Control 1)	21.73 ± 2.08	27.34 ± 2.16
EFgel formulation (Control 2)	17.82 ± 1.26*	22.43 ± 1.43*
EFNSgel formulation (Test 1)	6.89 ± 0.56**	7.32 ± 0.68**

Each value is the mean±S.D. of three determinations. *Significant statistical difference compared to control 1 ($p < 0.05$). ** Significant statistical difference compared to control 2 ($p < 0.05$)

The investigation into *in-vitro* skin permeation involved the assessment of NS-encapsulated efinaconazole gel formulations, with a Carbopol gel formulation containing free efinaconazole as the control counterpart. This experimental setup aimed to ascertain whether the observed enhancement in skin permeation was solely attributed to the gel formulation. As part of this exploration, skin permeation studies were also conducted using free efinaconazole dissolved in propylene glycol. In the context of our study, samples were extracted from the receptor media at specific time intervals (0.5, 1, 2, 4, 6, 8, 10, and 12 hours) to monitor potential transdermal delivery of efinaconazole. It is noteworthy that no trace of efinaconazole was detected in the receptor phase after the 12-hour application duration of both the control and the test formulations. This outcome indicates a lack of significant transdermal delivery of efinaconazole in the context of this study. Therefore, it can be inferred that the formulations, despite their variations, did not facilitate substantial penetration of efinaconazole through the skin over the given time frame.

Upon completion of the 12-hour permeation study, an assessment was made regarding the quantity of efinaconazole that had permeated and been deposited within the SC as well as the epidermis and dermis layers of the rat skin. Comparative analysis revealed that, in contrast to the efinaconazole solution in propylene glycol, both the Carbopol gel formulations containing encapsulated and non-encapsulated efinaconazole exhibited a significant enhancement in efinaconazole penetration into the skin 12 hours post-application. Specifically, the cumulative quantities of efinaconazole observed from the propylene glycol solution and the Carbopol gel formulation EFgel after the 12-hour dosing period were 6.74 ± 0.53 µg/cm² and 10.25 ± 0.92 µg/cm², respectively. In simpler terms, the cumulative quantity of efinaconazole that permeated the skin from the free efinaconazole gel formulation was approximately 1.52 times greater than that achieved through the propylene glycol solution within the same 12-hour timeframe. This difference highlights the significant impact of the gel formulation on the enhancement of efinaconazole skin penetration capabilities.

When comparing the Carbopol gel formulations of free efinaconazole, gel formulation containing encapsulated efinaconazole exhibited a substantial increase in efinaconazole skin penetration capabilities 12 hours after application. Specifically, the cumulative amounts of efinaconazole from the Carbopol gel formulations (EFgel, EFNSgel) at the 12-hour mark after dosing were measured at 10.25 ± 0.92 µg/cm² and 32.18 ± 1.43 µg/cm², respectively. This indicates that the cumulative amount of efinaconazole penetrating through the skin from the gel formulation containing encapsulated efinaconazole was over 3.14 times greater than that from the gel formulation containing

free efinaconazole within the same 12-hour timeframe. Notably, the gel formulation with NS-encapsulated efinaconazole demonstrated a fivefold increase in permeation through the skin compared to efinaconazole in propylene glycol.

In Figures 4C and 4D, we present the distribution pattern of efinaconazole within the excised rat skin. The time-course analysis of *in-vitro* efinaconazole skin penetration revealed a significant enhancement in its concentration within the SC at 3 hours, 6 hours, 9 hours, and 12 hours post-application when efinaconazole was incorporated within the NS. Similarly, the concentration of efinaconazole within the epidermis/dermis [(E + D)] also experienced significant enhancement at these time intervals ($p < 0.05$). This heightened permeation and deposition of efinaconazole can be attributed to the combined effects of NS encapsulation and the penetration-enhancing attributes of the Carbopol gel formulation. This underscores the potential synergy between NS and the gel base in enhancing efinaconazole skin penetration capabilities.

CONCLUSION

In this study, the optimization and characterization of HCDs were undertaken to enhance the delivery of efinaconazole in topical hydrogel formulations. Utilizing a Taguchi statistical design approach, critical parameters influencing HCD synthesis, such as reaction time, reaction temperature, stirring speed, and solvent volume, were systematically explored and optimized to create HCDs with a nanosponge-like structure. Characterization studies, including FTIR spectroscopy, XRPD, and DSC, validated the stability and suitability of HCDs as carriers. EFNS were successfully synthesized and characterized, confirming the formation of inclusion complexes between efinaconazole and HCDs, contributing to improved drug stability. These NS exhibited enhanced drug release profiles, showcasing a controlled release mechanism. When incorporated into a hydrogel, the formulation exhibited skin-compatible pH and enhanced photostability of efinaconazole, making it suitable for topical application. In excised rat skin studies, the hydrogel containing EFNS significantly improved drug penetration, indicating enhanced transdermal delivery. This study highlights the potential of HCDs as effective carriers for efinaconazole, offering controlled release, improved stability, and enhanced transdermal delivery for the development of more effective topical antifungal treatments.

AUTHOR CONTRIBUTIONS

Rudroju Anusha carried out the entire research and prepared the manuscript. Mothilal Mohan was involved in the analysis of the entire data and guided and reviewed the project from time to time.

FUNDING

There is no funding to report.

CONFLICTS OF INTEREST

The authors report no financial or any other conflicts of interest in this work.

ETHICAL APPROVAL

All animal experiments adhered to the approved protocols of the Institutional Animal Ethics Committee of TRR College of Pharmacy, with approval number 1447/PO/Re/S/11/CPCSEA-67/A. These stringent ethical guidelines were observed to ensure the welfare and ethical treatment of the animals throughout the experimentation process.

DATA AVAILABILITY

All the data is available with the authors and shall be provided upon request.

PUBLISHER'S NOTE

All claims expressed in this article are solely those of the authors and do not necessarily represent those of the publisher, the editors and the reviewers. This journal remains neutral with regard to jurisdictional claims in published institutional affiliation.

USE OF ARTIFICIAL INTELLIGENCE (AI)-ASSISTED TECHNOLOGY

The authors declares that they have not used artificial intelligence (AI)-tools for writing and editing of the manuscript, and no images were manipulated using AI.

CONSENT FOR PUBLICATION

This work is original and not published or under consideration in any other journal.

REFERENCES

1. Campoy S, Adrio JL. Antifungals. Biochem Pharmacol. 2017;133:86–6. doi: https://doi.org/10.1016/j.bcp.2016.11.019
2. Gupta AK, Stec N, Summerbell RC, Shear NH, Piguet V, Tosti A, *et al.* Onychomycosis: a review. J Eur Acad Dermatol Venereol. 2020;34(9):1972–90. doi: https://doi.org/10.1111/jdv.16394
3. Shahid SK. Newer patents in antimycotic therapy. Pharm Pat Anal. 2016;5(2):115–34. doi: https://doi.org/10.4155/ppa-2015-0001
4. Almuqbil RM, Sreeharsha N, Nair AB. Formulation-by-design of efinaconazole spanlastic nanovesicles for transungual delivery using statistical risk management and multivariate analytical techniques. Pharmaceutics. 2022;14(7):1419. doi: https://doi.org/10.3390/pharmaceutics14071419
5. Lee BC, Pangeni R, Na J, Koo KT, Park JW. Preparation and *in vivo* evaluation of a highly skin-and nail-permeable efinaconazole topical formulation for enhanced treatment of onychomycosis. Drug Deliv. 2019;26(1):1167–77. doi: https://doi.org/10.1080/10717544.2019.1687612
6. Agrawal V, Patel R, Patel M, Thanki K, Mishra S. Design and evaluation of microemulsion-based efinaconazole formulations for targeted treatment of onychomycosis through transungual route: *ex vivo* and nail clipping studies. Colloids Surf B. 2021;201:111652. doi: https://doi.org/10.1016/j.colsurfb.2021.111652
7. Verma S, Utreja P. Vesicular nanocarrier based treatment of skin fungal infections: potential and emerging trends in nanoscale pharmacotherapy. Asian J Pharm Sci. 2019;14(2):117–29. doi: https://doi.org/10.1016/j.ajps.2018.05.007
8. Garg A, Sharma GS, Goyal AK, Ghosh G, Si SC, Rath G. Recent advances in topical carriers of anti-fungal agents. Heliyon. 2020;6(8):e04663. doi: https://doi.org/10.1016/j.heliyon.2020.e04663
9. Felton T, Troke PF, Hope WW. Tissue penetration of antifungal agents. Clin Microbiol Rev. 2014;27(1):68–88. doi: https://doi.org/10.1128/cmr.00046-13
10. Saokham P, Muankaew C, Jansook P, Loftsson T. Solubility of cyclodextrins and drug/cyclodextrin complexes. Molecules. 2018;23(5):1161. doi: https://doi.org/10.3390/molecules23051161

11. Muller WW, Brauns U, inventors; Janssen Pharmaceutica NV, assignee. Pharmaceutical compositions containing drugs which are instable or sparingly soluble in water and methods for their preparation. Patent WO. 1985;85:02767.
12. Utzeri G, Matias P, Murtinho D, Valente AJ. Cyclodextrin-based NS: overview and opportunities. Front Chem. 2022;10:859406. doi: https://doi.org/10.3389/fchem.2022.859406
13. Girigoswami A, Girigoswami K. Versatile applications of NS in biomedical field: a glimpse on SARS-CoV-2 management. Bio Nano Science. 2022;12(3):1018–31. doi: https://doi.org/10.1007/s12668-022-01000-1
14. Selvamuthukumar S, Anandam S, Krishnamoorthy K, Rajappan M. NS: a novel class of drug delivery system-review. J Pharm Pharm Sci. 2012;15(1):103–11. doi: https://doi.org/10.18433/J3K308
15. Tiwari K, Bhattacharya S. The ascension of NS as a drug delivery carrier: preparation, characterization, and applications. J Mater Sci Mater Med. 2022;33(3):28. doi: https://doi.org/10.1007/s10856-022-06652-9
16. Ahmed MM, Fatima F, Anwer MK, Ibnouf EO, Kalam MA, Alshamsan A, *et al.* Formulation and *in vitro* evaluation of topical nanosponge-based gel containing butenafine for the treatment of fungal skin infection. Saudi Pharm J. 2021;29(5):467–77. doi: https://doi.org/10.1016/j.jsps.2021.04.010
17. Srivastava S, Mahor A, Singh G, Bansal K, Singh PP, Gupta R, *et al.* Formulation development, *in vitro* and *in vivo* evaluation of topical hydrogel formulation of econazole nitrate-loaded β-cyclodextrin NS. J Pharm Sci. 2021;110(11):3702–14. doi: https://doi.org/10.1016/j.xphs.2021.07.008
18. Aldawsari HM, Badr-Eldin SM, Labib GS, El-Kamel AH. Design and formulation of a topical hydrogel integrating lemongrass-loaded NS with an enhanced antifungal effect: *in vitro*/*in vivo* evaluation. Int J Nanomedicine. 2015;10:893–902. doi: https://doi.org/10.2147/IJN.S74771
19. Ferro M, Castiglione F, Punta C, Melone L, Panzeri W, Rossi B, *et al.* Anomalous diffusion of ibuprofen in cyclodextrin nanosponge hydrogels: an HRMAS NMR study. Beilstein J Org Chem. 2014;10(1):2715–23. doi: https://doi.org/10.3762/bjoc.10.286
20. Argenziano M, Haimhoffer A, Bastiancich C, Jicsinszky L, Caldera F, Trotta F, *et al. In vitro* enhanced skin permeation and retention of imiquimod loaded in β-cyclodextrin nanosponge hydrogel. Pharmaceutics. 2019;11(3):138. doi: https://doi.org/10.3390/pharmaceutics11030138
21. Huangs ML, Hung YH, Yang ZS. Validation of a method using Taguchi, response surface, neural network, and genetic algorithm. Measurement. 2016;94:284–94. doi: htpps://doi.org/10.1016/j.measurement.2016.08.006
22. Singireddy A, Pedireddi SR, Nimmagadda S, Subramanian S. Beneficial effects of microwave-assisted heating versus conventional heating in the synthesis of cyclodextrin-based NS. Mater Today Proc. 2016;3(10):3951–9. doi: https://doi.org/10.1016/j.matpr.2016.11.055
23. Singireddy A, Subramanian S. Cyclodextrin NS to enhance the dissolution profile of quercetin by inclusion complex formation. Part Sci Technol. 2016;34(3):341–6. doi: https://doi.org/10.1080/02726351.2015.1081658
24. Pedireddi S, Singireddy A, Varma MM, Jayanthi VR. Differential properties of nanoporous NS prepared from β-Cyclodextrin and 2-Hydroxypropyl β-Cyclodextrin. Adv Sci Eng Med. 2019;11(9):823–35. doi: https://doi.org/10.1166/asem.2019.2423
25. Kumar S, Prasad M, Rao R. Topical delivery of clobetasol propionate loaded nanosponge hydrogel for effective treatment of psoriasis: formulation, physicochemical characterization, antipsoriatic potential, and biochemical estimation. Mater Sci Eng. 2021;119:111605. doi: https://doi.org/10.1016/j.msec.2020.111605
26. Asad MI, Khan D, Rehman AU, Elaissari A, Ahmed N. Development and in vitro/in vivo evaluation of pH-sensitive polymeric nanoparticles loaded hydrogel for the management of psoriasis. Nanomaterials. 2021;11(12):3433. doi: htpps://doi.org/10.3390/nano11123433
27. Anandam S, Selvamuthukumar S. Fabrication of cyclodextrin NS for quercetin delivery: physicochemical characterization, photostability, and antioxidant effects. J Mater Sci. 2014;49:8140–53. doi: https://doi.org/10.1007/s10853-014-8523-6
28. Venuti V, Rossi B, Mele A, Melone L, Punta C, Majolino D, *et al.* Tuning structural parameters for the optimization of drug delivery performance of cyclodextrin-based NS. Expert Opin Drug Deliv. 2017;14(3):331–40. doi: https://doi.org/10.1080/17425247.2016.1215301
29. Wavikar P, Vavia P. Nanolipidgel for enhanced skin deposition and improved antifungal activity. AAPS pharmscitech. 2013;14:222–33. doi: https://doi.org/ 10.1208/s12249-012-9908-y
30. Kim KT, Kim JS, Kim MH, Park JH, Lee JY, Lee W, *et al.* Effect of enhancers on *in vitro* and *in vivo* skin permeation and deposition of S-Methyl-L-Methionine. Biomol Ther. 2017;25(4):434–40. doi: https://doi.org/10.4062/biomolther.2016.254
31. Singireddy A, Pedireddi SR, Subramanian S. Optimization of reaction parameters for synthesis of Cyclodextrin NS in controlled nanoscopic size dimensions. J Polym Res. 2019;26:1–2. doi: https://doi.org/10.1007/s10965-019-1754-0
32. Anandam S, Selvamuthukumar S. Optimization of microwave-assisted synthesis of cyclodextrin NS using response surface methodology. J Porous Mater. 2014;21:1015–23. doi: https://doi.org/10.1007/s10934-014-9851-2
33. Chung YT, Ba-Abbad MM, Mohammad AW, Hairom NH, Benamor A. Synthesis of minimal-size ZnO nanoparticles through sol–gel method: taguchi design optimisation. Mater Des. 2015;87:780–7. doi: https://doi.org/10.1016/j.matdes.2015.07.040
34. Dahl JA, Maddux BL, Hutchison JE. Toward greener nanosynthesis. Chem Rev. 2007;107(6):2228–69. doi: htpps://doi.org/10.1021/cr050943k
35. Chaudhary H, Kumar V. Taguchi design for optimization and development of antibacterial drug-loaded PLGA nanoparticles. Int J Biol Macromol. 2014;64:99–105. doi: https://doi.org/10.1016/j.ijbiomac.2013.11.032
36. Pungaiah SS, Kailasanathan CK. Thermal analysis and optimization of nano-coated radiator tubes using computational fluid dynamics and taguchi method. Coatings. 2020;10(9):804. doi: https://doi.org/10.3390/coatings10090804
37. Lee JU, Lee SS, Lee S, Oh HB. Noncovalent complexes of cyclodextrin with small organic molecules: Applications and insights into host–guest interactions in the gas phase and condensed phase. Molecules. 2020;25(18):4048. doi: https://doi.org/10.3390/molecules25184048

How to cite this article:
Anusha R, Mohan M. Optimization and characterization of hyper cross-linked cyclodextrins for improved efinaconazole delivery: A comprehensive study. J Appl Pharm Sci. 2024;14(08):216–229.